Nano Research
https://doi.org/10.1007/s12274-018-1989-9
Research Article
ISSN 1998-0124
CN 11-5974/O4

Liquid-FEP-based U-tube triboelectric nanogenerator for harvesting water-wave energy

Lun Pan[1,2,3,§], Jiyu Wang[1,§], Peihong Wang[1], Ruijie Gao[2,3], Yi-Cheng Wang[1], Xiangwen Zhang[2,3], Ji-Jun Zou[2,3], and Zhong Lin Wang[1,4] (✉)

[1] *School of Material Science and Engineering, Georgia Institute of Technology, Atlanta, Georgia 30332, USA*
[2] *Key Laboratory for Green Chemical Technology of the Ministry of Education, School of Chemical Engineering and Technology, Tianjin University, Tianjin 300072, China*
[3] *Collaborative Innovative Center of Chemical Science and Engineering (Tianjin), Tianjin 300072, China*
[4] *Beijing Institute of Nanoenergy and Nanosystems, Chinese Academy of Sciences, Beijing 100083, China*
[§] *Lun Pan and Jiyu Wang contributed equally to this work.*

Received: 21 November 2017
Revised: 24 December 2017
Accepted: 6 January 2018

KEYWORDS

triboelectric nanogenerator,
FEP U tube,
liquid properties,
ionic aqueous solution,
water-wave energy

ABSTRACT

Harvesting ambient mechanical energy is a key technology for realizing self-powered electronics. With advantages of stability and durability, a liquid–solid-based triboelectric nanogenerator (TENG) has recently drawn much attention. However, the impacts of liquid properties on the TENG performance and the related working principle are still unclear. We assembled herein a U-tube TENG based on the liquid–solid mode and applied 11 liquids to study the effects of liquid properties on the TENG output performance. The results confirmed that the key factors influencing the output are polarity, dielectric constant, and affinity to fluorinated ethylene propylene (FEP). Among the 11 liquids, the pure water-based U-tube TENG exhibited the best output with an open-circuit voltage (V_{oc}) of 81.7 V and a short-circuit current (I_{sc}) of 0.26 μA for the shaking mode (0.5 Hz), which can further increase to 93.0 V and 0.48 μA, respectively, for the horizontal shifting mode (1.25 Hz). The U-tube TENG can be utilized as a self-powered concentration sensor (component concentration or metal ion concentration) for an aqueous solution with an accuracy higher than 92%. Finally, an upgraded sandwich-like water-FEP U-tube TENG was applied to harvest water-wave energy, showing a high output with V_{oc} of 350 V, I_{sc} of 1.75 μA, and power density of 2.04 W/m^3. We successfully lighted up 60 LEDs and powered a temperature–humidity meter. Given its high output performance, the water-FEP U-tube TENG is a very promising approach for harvesting water-wave energy for self-powered electronics.

1 Introduction

With the increase of serious environment and energy-related issues around the world over the past decades, searching for sustainable and benign energy sources has been a major challenge facing today's society. Different from the needs of mega- to giga-watt power scales for solar, wind, and tide energies, the invention

Address correspondence to zhong.wang@mse.gatech.edu

of the smart triboelectric nanogenerator (TENG) by Wang's group in 2012 brought up abundant novel approaches to capture all kinds of mechanical energies available, but wasted, in our daily life or in nature [1], such as human motion, walking, vibration, mechanical triggering, wind, water flowing, ocean energy [1–11]. TENG is based on the combination of contact electrification and electrostatic induction [12]: Using the electrostatic charges created on the surfaces of two dissimilar materials when they are brought into physical contact, the contact-induced triboelectric charges can generate a potential drop when the two surfaces are separated by mechanical force, which can drive electrons to flow between the two electrodes built on each side surface [6].

Four fundamental working modes of TENG were invented, namely vertical contact–separation mode, lateral sliding mode, single-electrode mode, and free-standing mode [6]. Moreover, various prototypes, structures, and functions of TENGs based on the solid–solid frictions were reported [12–16]. The created charges via friction were closely dependent on the difference of ability to lose and gain electrons after the friction process [13]. In addition, many related materials were developed or modified to further modulate the surface electrostatic charges for special applications [6, 12–15, 17, 18]. Nevertheless, the performance of the solid–solid TENG could be sensitive to environmental factors, especially air humidity, resulting in the instability of the output values of TENG without encapsulation [19]. The physical collision with wear abrasion is another problem that must be settled for solid–solid frictions [20]. Alternatively, liquid–solid-mode TENGs have drawn much attention for their relatively stable output and durability [20–24]. In a liquid–solid TENG, the liquid with changeable shapes usually works as a positive triboelectric material to provide total contact with the solid friction layer to generate more electrostatic charges for a higher output performance [20, 25–27]. Furthermore, the flexible and flowing properties of liquids make them a lubricant for contact, resulting in good wear resistance and durability [20]. A few liquid-based TENGs were recently developed with working modes of contact–separation [25–28] and rotational type [29]. However, the inherent impact of liquid properties and the additive in liquid on the output performance of a liquid–solid TENG are rarely reported.

We assembled herein a facile U-tube TENG based on the liquid–solid mode, then applied 11 kinds of liquid to study the effect of liquid properties on the U-tube TENG output. The output was positively correlated with polarity, dielectric constant, and contact angle. Among these liquids, the pure water-based U-tube TENG delivered the best output, with an open-circuit V_{oc} of 81.7 V and I_{sc} of 0.26 μA for the shaking mode and V_{oc} of 93.0 V and I_{sc} of 0.48 μA for the horizontal shifting mode. Finally, an assembled sandwich-like U-tube TENG was utilized to harvest water-wave energy, showing a high output with V_{oc} of 350 V, I_{sc} of 1.75 μA, and a power density of 2.04 W/m^3, indicating its potential application in harvesting Blue Energy.

2 Results and discussion

2.1 Structure and working principle of the U-tube TENG

As illustrated in Fig. 1(a), a U-tube liquid-fluorinated ethylene propylene (FEP)-type TENG was assembled with three parts: FEP U-tube, Cu electrode, and liquid solution. FEP was chosen as the solid part because it is almost the best electronegative material with pure carbon-fluorine structure and full fluorination [6, 13]. The SEM image shows the inner surface of the FEP U-tube possessing a coarse nanostructure, which benefits the contact between the flowing liquid and the FEP inner surface. The liquid solution flowing in the inner surface of the FEP tube is the vital factor for inducing the separation of the electrons and the positive charges in the FEP and liquid solution, respectively [30]. Based on the flowing process of the positively charged liquid, the working mechanism of the U-tube TENG and the distribution of the electrical potential on the interface between the liquid (using water as example) and the FEP were simulated by COMSOL software using the finite element method and exhibited in Figs. 1(b) and 1(c) based on the freestanding model with three major steps involved [6].

At the first step (i), the positive charges in the liquid equaled that of the contacted FEP surface when the freestanding positively charged liquid approached the left side of the FEP U-tube, resulting in a very less charge generated on the surrounding left Cu electrode. Meanwhile, no liquid neutralized the negative charge

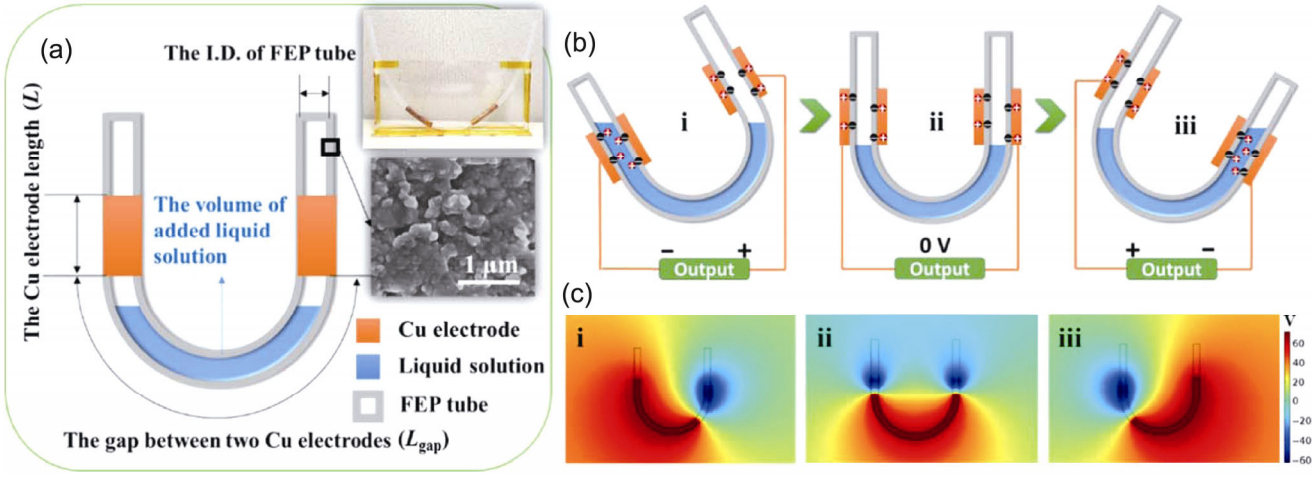

Figure 1 Structure design and working mechanism of the U-tube TENG. (a) Schematic illustration of the functional components of the U-tube TENG. (b) Simulated potential distribution and (c) working principle (between FEP surface and liquid, simulated by COMSOL software) under different U-tube TENG positions.

of the right FEP part, leading to an obvious accumulation of the positive charges on the surrounding right Cu electrode. Accordingly, a high electric potential was generated on the right electrode. With the gradual right rolling of the U tube, the liquid covering the area of the left Cu electrode decreased, while that of the right Cu electrode increased. Therefore, the transfer of the positive charges happened from the right Cu electrode to the left one, causing a gradually increased current with the direction from the right to the left, which will reach the highest in position (ii). However, the electrical potential difference between the two electrodes was zero. On the contrary, the further right rolling of the U tube will drive the positively charged liquid to overlap the FEP tube surrounded by the right Cu electrode and become far from the left Cu electrode. Hence, a high electric potential on the left electrode was generated in stage (iii). In the same manner, the positive charges would flow from the left to the right electrode, forming a reverse current through the external load, when the U tube continues to roll from the right side to the left side.

2.2 U-tube TENG optimization

The U-tube TENG output was closely related to the overlap position and the separation of the charged liquid and the FEP tube (Fig. 1(c)); thus, a parameter optimization was conducted. A shaker was applied to support the sway of the liquid–solid U-tube TENG, which produced the alternating current on the external load. The FEP tube inner diameter (I.D.) was first tuned using acetone as the model liquid. Figures 2(a) and 2(b) show that the open-circuit voltage (V_{oc}) and the transferred charge (Q) are 2.3 V and 0.8 nC, respectively, when I.D. is 4 mm. Importantly, more than 2 times of V_{oc} and Q promotion was observed for I.D. = 6 and 8 mm, respectively, while they gradually decreased with a further large I.D. of 10 mm. The V_{oc} and Q normalization by the cross-sectional area of the FEP tube was then analyzed (Fig. 2(c)), confirming the better output performance of the U-tube TENG with an I.D. = 6 mm. The larger-diameter TENG had a relatively poor output performance because of the better fluidity, which will make it difficult for water to completely fill the cross-sectional area of the FEP tubes. Therefore, I.D. = 6 mm was applied for all the following tests.

Aside from the interaction between the positively charged liquid and the negatively charged FEP tube, the final output of the U-tube TENG was generated from the electrostatic induction of the surrounding Cu electrodes (Fig. 1(b)) [20, 31]. Hence, the length of the Cu electrodes (L) and their gap (L_{gap}) were modulated (marked in Fig. 1(a)) and accompanied with a tunable liquid volume (V_{liquid} or corresponding liquid length in the U tube) (Figs. 2(d) and 2(e)). Fixing the length of the Cu electrodes (L) to 6 cm, the output V_{oc} was approximately 1.5 V when L_{gap} = 1 cm and V_{liquid} = 1 mL. The output then gradually increased with the increase of L_{gap} and V_{liquid} and reached the maximum of 5.7 V

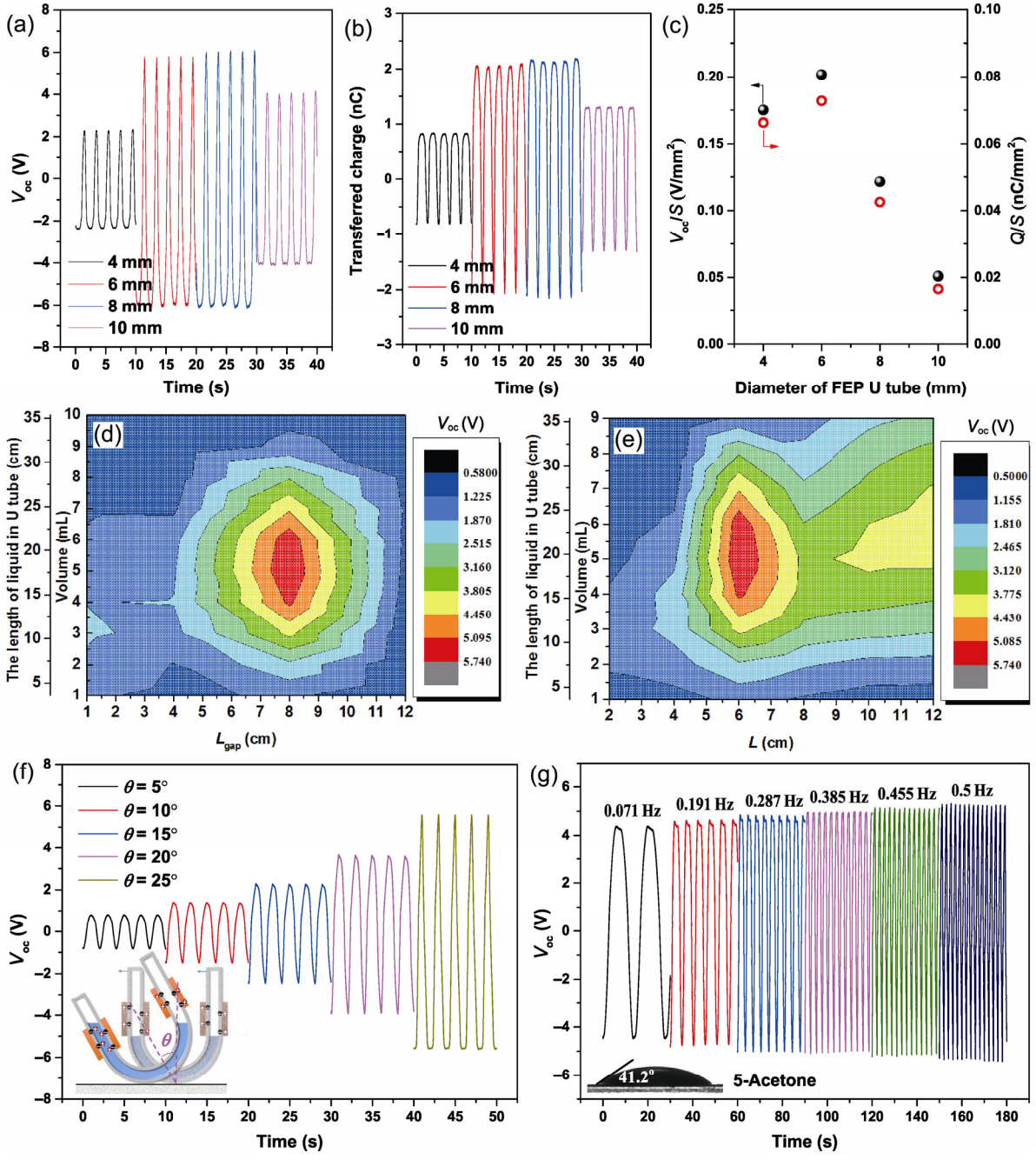

Figure 2 Parameter modulation of the U-tube TENG using acetone as the model liquid to optimize its output on the shaker. (a) V_{oc} and (b) Q of the U-tube TENG with different FEP I.D. (c) Normalized V_{oc} and Q by cross-sectional area. (d) Gap between two Cu electrodes (L_{gap}) and (e) length of the Cu electrode (L) accompanied with a tunable liquid volume. (f) Amplitude and (g) frequency of the shaker.

when L_{gap} = 8 cm and V_{liquid} = 5 mL. However, a further increase of L_{gap} and V_{liquid} will decline the U-tube TENG output because of the reduced area for electrostatic induction on the Cu electrode via an excessive overlap of the charge liquid and the FEP tube [27]. Furthermore, fixing L_{gap} = 8 cm, L and V_{liquid} were tuned to optimize the output (Fig. 2(e)). Similarly, for the highest U-tube TENG output, the optimal L was 6 cm, and V_{liquid} was 5 mL. Therefore, the optimal parameters for this liquid-FEP U-tube TENG were L_{gap} = 8 cm, L = 6 cm, and V_{liquid} = 5 mL. These values were applied for all the tests that follow.

The effects of the amplitude and the sway frequency of the shaker on the output were also investigated (Figs. 2(f) and 2(g)). Both the high amplitude and sway

frequency benefitted the output. However, the amplitude had a significant impact on V_{oc} (i.e., 5.5-times rise with a rolling angle from 5° to 25°), while the effect was limited for the sway frequency (i.e., only a 1.2-times rise with a frequency from 0.071 Hz to 0.5 Hz) because the latter had less effect on the overlap between the liquid and the Cu electrodes. With the rolling angle changing from 5° to 25°, the liquid can totally overlap the Cu electrode on one side, while the liquid will separate from the Cu electrode on the other side. As shown in Fig. S1 in the Electronic Supplementary Material (ESM), the separated distance between the liquid and the electrode illustrated a direct proportion on the final output, with the total separation occurring for $\theta = 25°$.

2.3 Impacts of liquid properties on the TENG output performance

We utilized 11 kinds of liquids in the U-tube TENG, namely 1-hexane, 2-ether, 3-chlorobenzene, 4-isopropanol, 5-acetone, 6-ethanol, 7-*N*,*N*-dimethylformamide, 8-acetonitrile, 9-ethylene glycol, 10-dimethyl sulfoxide (DMSO), and 11-water, to investigate the effects of the liquid inherent properties on the TENG output performance. Figure 3(a) presents the output performance. The output performances for liquids 1 to 3 were very low, while the V_{oc} output from liquids 4 to 11 gradually increased. Among them, the pure water-FEP U-tube TENG exhibited the best performance with V_{oc} of 66.4 V in a frequency of 0.071 Hz (Fig. 3).

As reported, the voltage V for the dielectric-to-dielectric sliding-mode TENG can be estimated by Eq. (1) [32]

$$V = \sigma\omega\upsilon R \ln\left(\frac{l-\upsilon t}{l}\right) \quad (1)$$

where σ is the tribo-charge surface density; and ω, l,

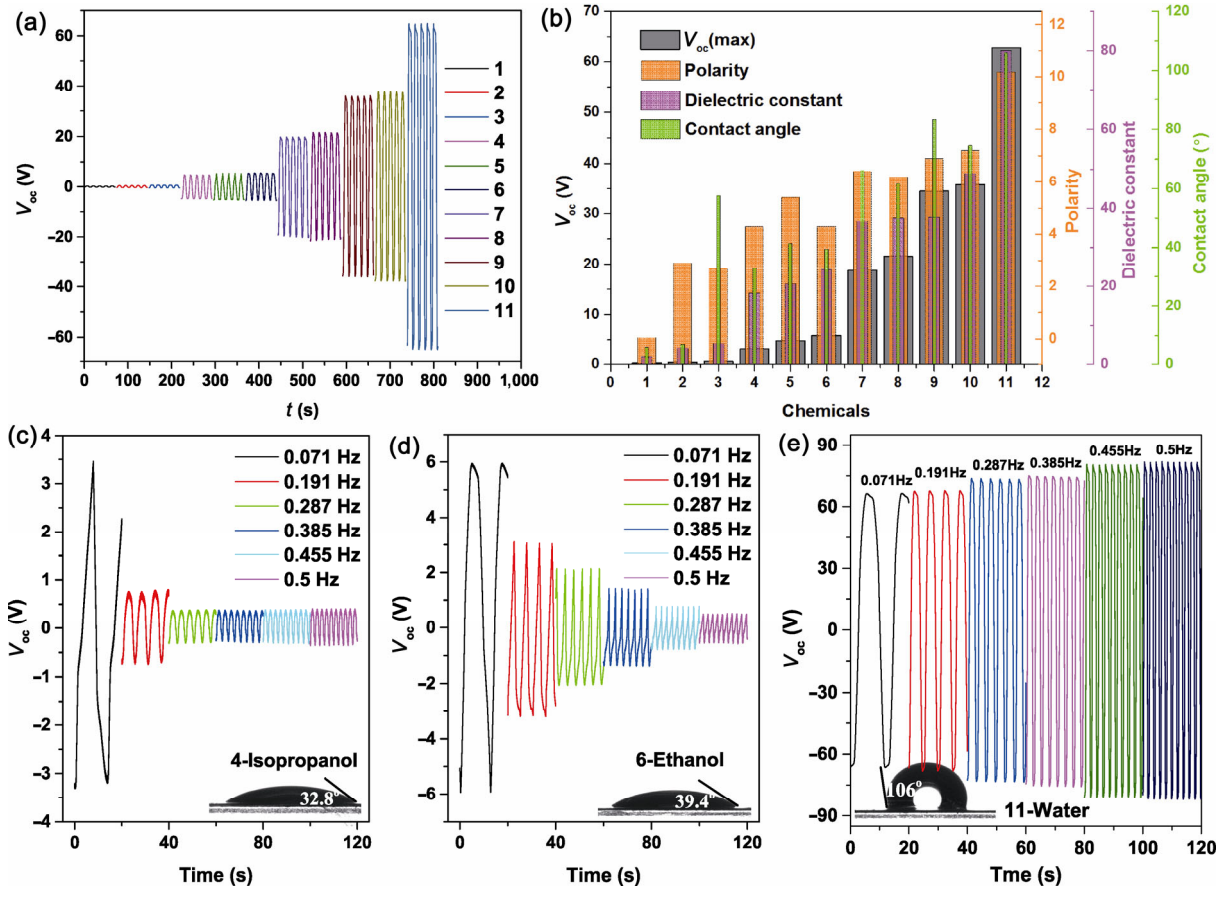

Figure 3 Impact of liquid properties on the liquid-FEP U-tube TENG output performance. (a) V_{oc} of 11 types of liquid under a 0.071 Hz frequency; (b) relationship between V_{oc} and polarity/dielectric constant/contact angle (1-hexane; 2-ether; 3-chlorobenzene; 4-isopropanol; 5-acetone; 6-ethanol; 7-*N*,*N*-dimethylformamide; 8-acetonitrile; 9-ethylene glycol; 10-DMSO; 11-water); (c)–(e) frequency-dependent output of the U-tube TENG based on isopropanol, ethanol, and water, respectively.

and v are the dielectric width, dielectric length, and velocity, respectively. For the liquid-FEP U-tube TENG with fixed parameters (ω, l, and v), σ is the most important parameter for determining the output [25] closely dependent on the inherent liquid properties. Therefore, the possibly relevant liquid properties (i.e., polarity, dielectric constant, and contact angle) between the liquid drop and the FEP surface were investigated and exhibited in Fig. 3(b) and Figs. S2–S4 in the ESM. The V_{oc} output had a positive correlation with these three properties; however, the complex molecule structure of liquid cannot lead to the perfect correlation between V_{oc} and the liquid properties. Moreover, the apparent output performance of the U-tube TENG was co-affected by these three properties. For instance, 2-ether, which possessed a much higher polarity than 1-hexane, only had a comparative V_{oc} with the latter because of its very low contact angle. Although with a much higher contact angle, 3-chlorobenzene exhibited low polarity and dielectric constant, resulting in the poor output of the U-tube TENG. Furthermore, 7-*N*,*N*-dimethylformamide, 8-acetonitrile, and 9-ethylene glycol had similar dielectric constants. The much higher output of 9-ethylene glycol should be attributed to its much higher contact angle.

Importantly, the affinity to FEP (contact angle property) can significantly alter the liquid-FEP TENG output according to the change of the shaking frequency. Four typical liquids (i.e., 4-isopropanol, 5-acetone, 6-ethanol, and 11-water) were utilized to determine the effects of the affinity to FEP on the U-tube TENG output (Figs. 2(g) and 3(c)–3(e)). For 4-isopropanol and 6-ethanol, only a low 0.071 Hz frequency can produce the real output of the related U-tube TENG, while a high frequency above 0.191 Hz will cause the rapid decrease of V_{oc}. Different for 5-acetone and 11-water, the high frequency slightly benefits the output. These results indicated that the output should be closely related to the affinity to FEP because the contact angles for 4-isopropanol and 6-ethanol were below 39.4°, while higher contact angles were observed for 5-acetone (41.2°) and 11-water (106°). Figures 1(b) and 1(c) show that only under the total separation of liquid from the FEP surface (in the Cu electrode area) can the AC current be generated [27], which is under the theoretical condition without the liquid affinity to FEP. When the liquid possesses a higher affinity to FEP (e.g., isopropanol and ethanol), its flow will be delayed, and the retained positively charged liquid will compensate the negatively charged FEP, which will not lead to the charges on the Cu electrode and further AC current. Therefore, the contact angle above 41° is needed for the U-tube TENG assembly to prohibit the decrease of the output with the increase of the applied shaking frequency. In addition, for the liquids with a low affinity to FEP (e.g., 5-acetone and 11-water), the slightly enhanced output with the high frequency should be related to the increased friction force caused by the centrifugal force.

From the abovementioned results, note that the liquid with higher polarity, dielectric constant, and contact angle (between the liquid drop and the FEP surface) showed a higher output performance, and these three parameters can be used to choose the liquid type to construct specific liquid–solid TENG.

2.4 Applications of the U-tube TENG

2.4.1 *Self-powered concentration sensor for aqueous solution*

The U-tube TENG based on different liquids showed a greatly varied V_{oc}; thus, the output can be applied as a self-powered concentration sensor for the mixed liquid solution and the ionic aqueous solution. As shown in Fig. 4(a), when water is mixed with acetone, ethanol, isopropanol, or DMSO, the mixture exhibited distinct curves with the increase of the water volume content, with the DMSO–water curve above the dot line between the pure water and the pure DMSO and the acetone–water, ethanol–water, and isopropanol–water curves below their respective dot lines between the pure acetone/ethanol/isopropanol and the pure water directly related to the affinity to the FEP surface. With poor affinity to FEP, DMSO and water molecules both excluded the FEP surface, and no liquid residual was found on the FEP surface during shaking. The water output will then dominate the apparent output for its smaller molecule size, and the curve will be above the pure DMSO–pure water dot line. In contrast, acetone, ethanol, and isopropanol were very apt to adsorb on the FEP surface compared with water, and will leave a residue during shaking, which will contribute more to the low apparent output of the mixture. Therefore, the liquid affinity to FEP or other materials can be estimated from the mixture curve shape. We then tested the water

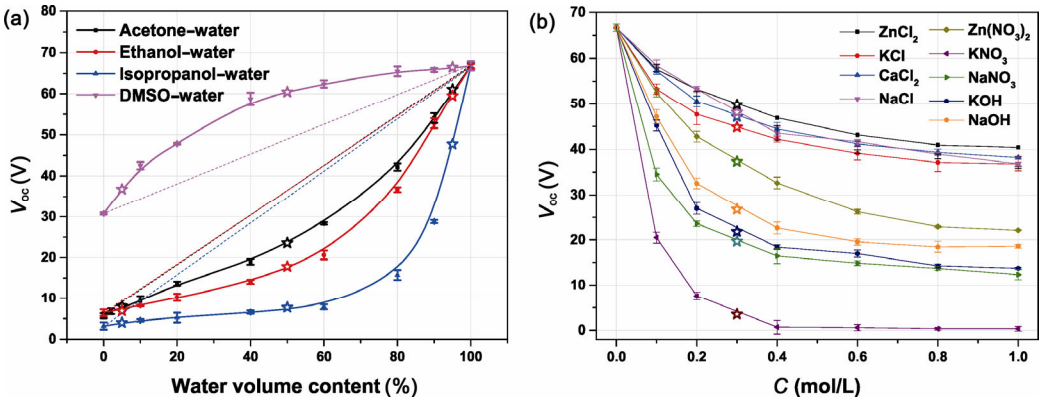

Figure 4 Application of the U-tube TENG as a self-powered concentration sensor. The U-tube TENG output based on the (a) mixed chemicals and (b) the ionic aqueous solution with 0.5 Hz frequency. The hollow stars denote the tested mixture solution.

volume concentration of 12 mixture solutions marked as hollow stars in Fig. 4(a). Importantly, all the tested samples were on the mixture curves (with the accuracy higher than 95%), indicating the U-tube TENG can be used for the self-power concentration sensor for the bi-liquid mixture.

Moreover, the effects of the ionic compounds on the performance of the water-based U-tube TENG were further investigated (Fig. 4(b)). Surprisingly, all added ionic compounds were harmful to the output of the water-FEP U-tube TENG. The addition of low-concentration (C) ionic compounds from 0.1 to 0.6 mol/L rapidly decreased V_{oc}, which became stable with a further higher C. With the same anion of Cl^-, the ionic compounds with different cations showed the output performance order of $Zn^{2+} > Ca^{2+} \approx Na^+ > K^+$, which should be correlated with their electronegativity properties (Zn, 1.65; Ca, 1.00; Na, 0.93; and K, 0.82). The cations with a low electronegativity preferred to electrostatically adsorb to the F^- groups on the FEP surface, resulting in the decline of the induced positive charges on the outer Cu electrode and a further low output [33]. Figure 4(b) also illustrates that, given the same cations of K^+, the performance order of the anions in the aqueous solution was $Cl^- > OH^- > NO_3^-$, which was related to their electrostatic force with the K^+ ions (a smaller ionic radius led to a higher electrostatic force if the charge was equal [34]). The KNO_3 with a much lower electrostatic force than K^+–F^- caused many K^+ ions to accumulate on the FEP tube surface. Moreover, its aqueous solution with C higher than 0.4 mol/L decreased the U-tube TENG output V_{oc} to ca. 0.63 V or less. Furthermore, this U-tube TENG can be used as a sensor to detect the ionic concentration in the aqueous solution. We tested five ionic solutions marked as hollow stars in Fig. 4(b). All the tested concentrations were located on the working curves with an accuracy higher than 92%, indicating that the U-tube TENG can also be used for the ionic concentration sensor.

2.4.2 *Water-wave energy (Blue Energy) harvesting*

Based on the abovementioned results, pure water was the best liquid choice among the tested 11 liquids and ionic aqueous solution to realize the highest liquid-FEP U-tube TENG output, which can be utilized to harvest water-wave-vibration energy (or Blue Energy). Accordingly, the pure water-FEP U-tube TENG was first applied to harvest mechanical energy in two modes: the shaking mode driven by a shaker (Figs. 5(a)–5(e)) and the shifting mode driven by a linear motor (Figs. 5(f)–5(k)). For the shaking mode, V_{oc} (and Q) of the U-tube TENG gradually increased from 66.4 to 81.7 V (Fig. 3(e) (from 21.6 to 28.9 nC, Fig. 5(a)) with the frequency raised from 0.071 to 0.5 Hz. Meanwhile, I_{sc} rapidly increased from 0.02 to 0.26 μA (Fig. 5(b)). We then utilized this shaking-mode TENG with a rectifier bridge to support 60 LEDs (Figs. 5(c)–5(e)). The rectification of the output double the frequency of the transferred charges and the current. Figure 5(d) shows that the frequency to initially light 60 LEDs was as low as 0.574 Hz, in which case, the current in the loop was 0.11 μA. Importantly, the loop current with the 60-LED load was almost similar to that with the short-circuit current (Figs. 5(b) and 5(e)), which can be attributed to the much lower electric resistance of 60 LEDs compared with the equivalent resistance of TENG. Video ESM1

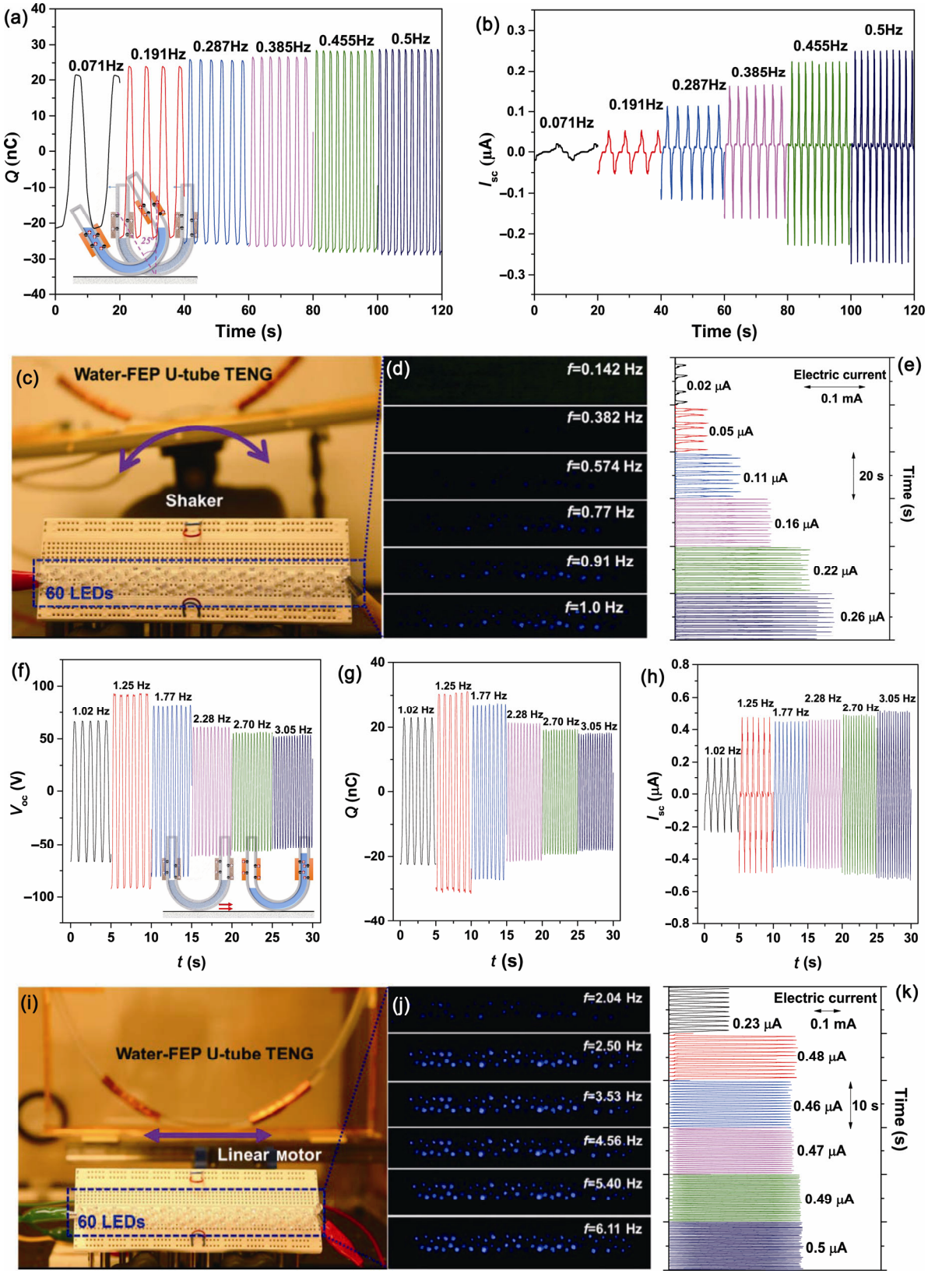

Figure 5 Output performance of the water-FEP U-tube TENG on the shaker (a)–(e) and the linear motor (f)–(k); (a) and (g) transferred charge; (b) and (h) short-circuit current; (f) open-circuit voltage; (c), (d), (i), and (j) photographs of lighting up the 60 LEDs; (e) and (k) corresponding electric current (the rectification of the output doubles the current frequency).

presents lighting up of 60 LEDs under a 1.0 Hz frequency.

For the U-tube TENG in the shifting mode driven by a linear motor (Figs. 5(f)–5(k)), V_{oc} and Q increased from 66.5 V and 23.1 nC to the maximum values of 93.0 V and 30.56 nC, respectively, with its frequency increased from 1.02 to 1.25 Hz (Figs. 5(f) and 5(g)). However, further increasing the frequency to 3.05 Hz gradually decreased V_{oc} and Q. Different from the shaking mode, the U-tube TENG output in the horizontal shifting mode can be significantly affected by the frequency. Figure S5 in the ESM shows that the V_{oc} curve with a 1.25 Hz frequency was in a ladder shape, which only appeared when the liquid level was completely lower than the Cu electrode in one side of the U tube during the shifting mode. However, a lower frequency (1.02 Hz) and a higher frequency (≥ 1.77 Hz) will shorten the liquid shift amplitude, and cannot realize the complete separation of the liquid and the Cu electrode, resulting in a pseudo-sine-like signal. As for I_{sc}, a great increase from 0.23 to 0.48 μA was observed with the frequency from 1.02 to 1.25 Hz (Fig. 5(h)), which was mainly contributed by the increased transferred charges. Nevertheless, no obvious decrease of I_{sc} was found with a further higher frequency (≥ 1.77 Hz). Meanwhile, a slight increase happened because the dominant contribution to I_{sc} was switched to the increased liquid flowing velocity and the decreased cycle.

We then utilized this shifting-mode TENG with a rectifier bridge to support 60 LEDs (Figs. 5(i)–5(k)). The rectification of the output doubled the output frequency. The loop current when the frequency was 2.04 Hz was 0.23 μA. The loop current with the 60-LED load was similar to that with the short-circuit current. Video ESM2 shows the lighting up of 60 LEDs under a 2.50 Hz frequency. From the abovementioned results, note that the liquid-FEP U-tube TENG can be used to harvest the shaking mechanical energy and the horizontal shifting energy, then convert them to a high-voltage electric power. This U-tube TENG also exhibited high stability and durability (Fig. S6 in the ESM).

A practical demonstration in the collection of the water-wave energy (or Blue Energy) was conducted (the used water is deionized water) herein to further explore the possible application of the developed water-FEP U-tube TENG. As shown in Fig. 6(a), the water-FEP U-tube TENG was placed in another FEP tube jacket (I.D. of 10 mm), forming a sandwich-like U-tube TENG, in which the induced charges on the Cu electrode were from both the inner water-FEP U-tube TENG and the outer U-tube TENG with the friction between the outer FEP tube and the outer water when driven by the water wave. Another important function of the outer FEP tube was preventing the contact between the Cu electrode and the outer water.

Five upgraded sandwich-like U-tube TENGs were then paralleled as the energy-harvesting and power-supply apparatus to drive 60 LEDs and the temperature–humidity meter. The water wave can drive this U-tube TENG moving in the shaking mode with a high energy and in the shifting mode with a relatively low energy. The optimal driven frequency for this device was 1.1 Hz, and V_{oc} and I_{sc} can achieve 350 V and 1.75 μA, respectively, with Q of 200 nC (Figs. 6(b)–6(d)). Figure 6(e) shows the output power and voltage with different external load resistances. The calculation method of the output power P is $P = U^2/R$, where U is the output voltage across the external load, and R is the load resistance. The voltage across the load increased with the external load resistance. The output power can reach a maximum of 0.24 mW when the external load resistance is ca. 200 MΩ, with a normalized power density of 2.04 W/m^3. Such a high output should be attributed to the extremely low friction coefficient and the large effective contacting surface of the liquid–solid contact [27].

The corresponding commercial LEDs and the temperature–humidity meter were lighted up when the TENG was driven by water wave (Figs. 6(f)–6(i)). Videos ESM3 and ESM4 show the demo videos. This kind of sandwich-like U-tube TENG is very promising to apply in harvesting water-wave or Blue Energy because it can simultaneously utilize the inner and outer water-FEP triboelectric energy for self-powered electronics.

3 Conclusion

In this work, a facile liquid–solid U-tube TENG was designed and constructed, in which 11 kinds of liquid were applied to study the effects of liquid properties on the output. Three factors (i.e. polarity, dielectric constant, and affinity to FEP) were found vital to the output. Among these liquids, the pure water-based U-tube TENG exhibited the best performance, delivering

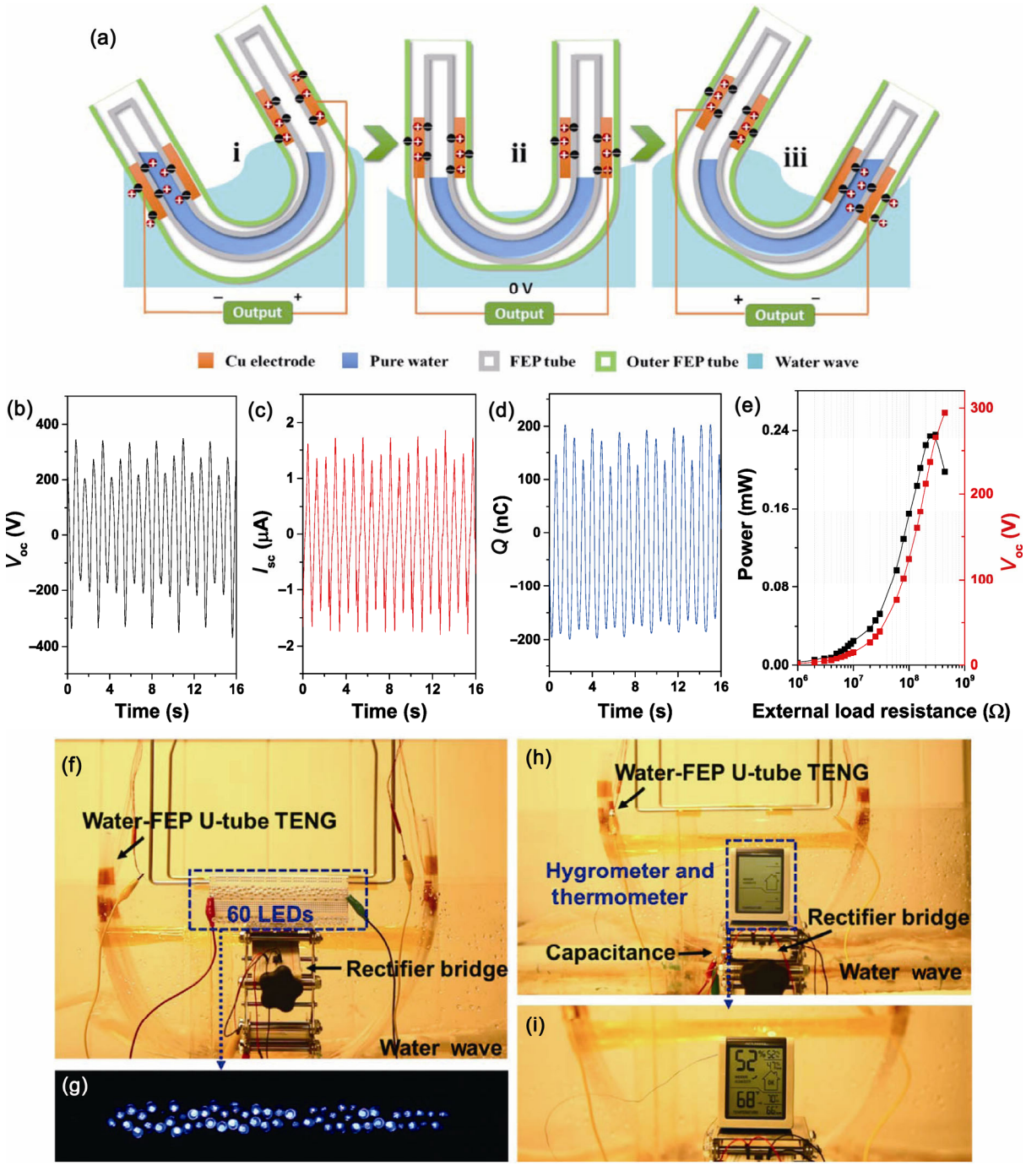

Figure 6 Output performance of the sandwich-like water-FEP U-tube TENGs driven by water wave for Blue Energy harvesting. (a) Schematic illustration of the functional components and working principle of the U-tube TENG; (b) open-circuit voltage; (c) short-circuit current; (d) transferred charges; (e) output peak power and voltage under varied external load resistances; photos of lighting LEDs (f) and (g); and driving the temperature–humidity meter ((h) and (i)). The water wave is driven by a linear motor with a frequency of 1.1 Hz (the output signal was tested after it remained stable, and the rectification of the output doubles the frequency of the current).

V_{oc} of 81.7 V and I_{sc} of 0.26 μA for the shaking mode (1.0 Hz), which can further increase to 93.0 V and 0.48 μA, respectively, for the horizontal shifting mode (1.25 Hz). This U-tube TENG can be utilized as a self-powered concentration sensor (component concentration or metal ion concentration) for an aqueous solution with an accuracy higher than 92%. Furthermore, we assembled an upgraded sandwich-like water-FEP U-tube TENG

and used it to harvest water-wave energy (or Blue Energy), showing a high output with V_{oc} of 350 V, I_{sc} of 1.75 μA, and a power density of 2.04 W/m^3. We successfully lighted up 60 LEDs and powered a temperature–humidity meter. This work provides a novel approach to improve the TENG output for Blue Energy harvesting.

4 Experimental section

4.1 Materials

Fluorinated ethylene propylene (FEP) and a highly conductive copper electrical tape with a conductive adhesive were obtained from McMaster-Carr. Hexane, ether, chlorobenzene, isopropanol, acetone, ethanol, *N*,*N*-dimethylformamide, acetonitrile, ethylene glycol, DMSO, $ZnCl_2$, $CaCl_2$, KCl, NaCl, $Zn(NO_3)_2$, KNO_3, $NaNO_3$, KOH, and NaOH were all purchased from Sigma-Aldrich. All materials or chemicals were used as received without any further purification unless mentioned elsewhere. Ultrapure water (≥ 18.2 MΩ·cm) was used in this work.

4.2 Fabrication of U-tube TENG

A 1.0 mm-thick FEP U-shaped tube with various inner diameters (I.D. = 4, 6, 8, and 10 mm) and very high polarity and transparency properties was selected to construct the U-tube TENG. Two conducting Cu tapes (88.5 μm thick) with a tunable length L (L = 2, 4, 6, 8, and 10 cm) and a gap length L_{gap} (L_{gap} = 2, 4, 6, 8, 10, and 12 cm) between each other were attached onto two columns of the FEP U-shaped tube. The liquid (1-hexane, 2-ether, 3-chlorobenzene, 4-isopropanol, 5-acetone, 6-ethanol, 7-*N*,*N*-dimethylformamide, 8-acetonitrile, 9-ethylene glycol, 10-DMSO, and 11-water) was then partially filled into the FEP U tube with a tunable volume V_{liquid} (V_{liquid} = 1–9 mL), and the liquid level was located in the center of the two Cu tapes. Finally, two leads were welded on to the two Cu electrodes to form the U-tube TENG (Fig. 1(a)).

4.3 Characterization and measurement

A Hitachi SU8010 field-emission SEM was used to measure the inner surface morphology of the FEP tube. A step motor (LinMot E1100) and an orbital shaker (Orbi-Blotter™ Benchmark) were applied to mimic the shaking and horizontal shifting movements of the U-tube TENG. A programmable electrometer (Keithley, model 6514) was adopted to test the open-circuit voltage (V_{oc}), short-circuit current (I_{sc}), and transferred charge (Q). The software platform was constructed based on LabView, which can realize a real-time data acquisition. A water wave was then mimicked powered by another linear motor (LinMot E1100) to test the potential application of the U-tube TENG in Blue Energy harvesting.

Acknowledgements

Research was supported by the KAUST, the Hightower Chair foundation, and the "thousands talents" program for pioneer researcher and his innovation team, China, the National Key R & D Project from the Ministry of Science and Technology (Nos. 2016YFA0202704 and 2016YFA0202702), the National Natural Science Foundation of China (Nos. 51432005, 5151101243, and 51561145021), and the Chinese Scholars Council.

Electronic Supplementary Material: Supplementary material (the effects of liquid properties, the stability of U-tube TENG, and so on) is available in the online version of this article at https://doi.org/10.1007/s12274-018-1989-9.

References

[1] Fan, F.-R.; Tian, Z.-Q.; Wang, Z. L. Flexible triboelectric generator. *Nano Energy* **2012**, *1*, 328–334.

[2] Wang, Z. L.; Jiang, T.; Xu, L. Toward the blue energy dream by triboelectric nanogenerator networks. *Nano Energy* **2017**, *39*, 9–23.

[3] Zi, Y. L.; Wang, Z. L. Nanogenerators: An emerging technology towards nanoenergy. *APL Mater.* **2017**, *5*, 074103.

[4] Wang, Z. L. Catch wave power in floating nets. *Nature* **2017**, *542*, 159–160.

[5] Wang, Z. L. On Maxwell's displacement current for energy and sensors: The origin of nanogenerators. *Mater. Today* **2017**, *20*, 74–82.

[6] Wang, Z. L.; Chen, J.; Lin, L. Progress in triboelectric nanogenerators as a new energy technology and self-powered sensors. *Energy Environ. Sci.* **2015**, *8*, 2250–2282.

[7] Dong, K.; Wang, Y.-C.; Deng, J.; Dai, Y. J.; Zhang, S. L.; Zou, H. Y.; Gu, B. H.; Sun, B. Z.; Wang, Z. L. A highly stretchable and washable all-yarn-based self-charging knitting power textile composed of fiber triboelectric nanogenerators and supercapacitors. *ACS Nano* **2017**, *11*, 9490–9499.

[8] Zhang, M.; Jie, Y.; Cao, X.; Bian, J.; Li, T.; Wang, N.; Wang, Z. L. Robust design of unearthed single-electrode TENG from three-dimensionally hybridized copper/polydimethylsiloxane film. *Nano Energy* **2016**, *30*, 155–161.

[9] Wen, Z.; Guo, H. Y.; Zi, Y. L.; Yeh, M.-H.; Wang, X.; Deng, J.; Wang, J.; Li, S. M.; Hu, C. G.; Zhu, L. P. et al. Harvesting broad frequency band blue energy by a triboelectric–electromagnetic hybrid nanogenerator. *ACS Nano* **2016**, *10*, 6526–6534.

[10] Yu, H.; He, X.; Ding, W. B.; Hu, Y. S.; Yang, D. C.; Lu, S.; Wu, C. S.; Zou, H. Y.; Liu, R. Y.; Lu, C. H. et al. A self-powered dynamic displacement monitoring system based on triboelectric accelerometer. *Adv. Energy Mater.* **2017**, *7*, 1700565.

[11] Li, Z. L.; Shen, J. L.; Abdalla, I.; Yu, J. Y.; Ding, B. Nanofibrous membrane constructed wearable triboelectric nanogenerator for high performance biomechanical energy harvesting. *Nano Energy* **2017**, *36*, 341–348.

[12] Wang, Z. L. Triboelectric nanogenerators as new energy technology for self-powered systems and as active mechanical and chemical sensors. *ACS Nano* **2013**, *7*, 9533–9557.

[13] Chen, J.; Wang, Z. L. Reviving vibration energy harvesting and self-powered sensing by a triboelectric nanogenerator. *Joule* **2017**, *1*, 480–521.

[14] He, C.; Han, C. B.; Gu, G. Q.; Jiang, T.; Chen, B. D.; Gao, Z. L.; Wang, Z. L. Hourglass triboelectric nanogenerator as a "direct current" power source. *Adv. Energy Mater.* **2017**, *7*, 1700644.

[15] Li, S. M.; Wang, J.; Peng, W. B.; Lin, L.; Zi, Y. L.; Wang, S. H.; Zhang, G.; Wang, Z. L. Sustainable energy source for wearable electronics based on multilayer elastomeric triboelectric nanogenerators. *Adv. Energy Mater.* **2017**, *7*, 1602832.

[16] Shen, J. L.; Li, Z. L.; Yu, J. Y.; Ding, B. Humidity-resisting triboelectric nanogenerator for high performance biomechanical energy harvesting. *Nano Energy* **2017**, *40*, 282–288.

[17] Wang, A. C.; Wu, C. S.; Pisignano, D.; Wang, Z. L.; Persano, L. Polymer nanogenerators: Opportunities and challenges for large-scale applications. *J. Appl. Polymer Sci.*, in press, DOI: 10.1002/app.45674.

[18] Li, Z. L.; Chen, J.; Zhou, J. J.; Zheng, L.; Pradel, K. C.; Fan, X.; Guo, H. Y.; Wen, Z.; Yeh, M.-H.; Yu, C. W. et al. High-efficiency ramie fiber degumming and self-powered degumming wastewater treatment using triboelectric nanogenerator. *Nano Energy* **2016**, *22*, 548–557.

[19] Nguyen, V.; Zhu, R.; Yang, R. S. Environmental effects on nanogenerators. *Nano Energy* **2015**, *14*, 49–61.

[20] Zhang, X. L.; Zheng, Y. B.; Wang, D. A.; Zhou, F. Solid-liquid triboelectrification in smart U-tube for multifunctional sensors. *Nano Energy* **2017**, *40*, 95–106.

[21] Seol, M.-L.; Jeon, S.-B.; Han, J.-W.; Choi, Y.-K. Ferrofluid-based triboelectric-electromagnetic hybrid generator for sensitive and sustainable vibration energy harvesting. *Nano Energy* **2017**, *31*, 233–238.

[22] Zhao, X. J.; Tian, J. J.; Kuang, S. Y.; Ouyang, H.; Yan, L.; Wang, Z. L.; Li, Z.; Zhu, G. Biocide-free antifouling on insulating surface by wave-driven triboelectrification-induced potential oscillation. *Adv. Mater. Interfaces* **2016**, *3*, 1600187.

[23] Chen, J.; Guo, H. Y.; Zheng, J. G.; Huang, Y. Z.; Liu, G. L.; Hu, C. G.; Wang, Z. L. Self-powered triboelectric micro liquid/gas flow sensor for microfluidics. *ACS Nano* **2016**, *10*, 8104–8112.

[24] Li, X. H.; Yeh, M.-H.; Lin, Z.-H.; Guo, H. Y.; Yang, P.-K.; Wang, J.; Wang, S. H.; Yu, R. M.; Zhang, T. J.; Wang, Z. L. Self-powered triboelectric nanosensor for microfluidics and cavity-confined solution chemistry. *ACS Nano* **2015**, *9*, 11056–11063.

[25] Lin, Z.-H.; Cheng, G.; Lin, L.; Lee, S.; Wang, Z. L. Water–solid surface contact electrification and its use for harvesting liquid-wave energy. *Angew. Chem. Int. Ed.* **2013**, *52*, 12545–12549.

[26] Lin, Z.-H.; Cheng, G.; Lee, S.; Pradel, K. C.; Wang, Z. L. Harvesting water drop energy by a sequential contact-electrification and electrostatic-induction process. *Adv. Mater.* **2014**, *26*, 4690–4696.

[27] Tang, W.; Jiang, T.; Fan, F. R.; Yu, A. F.; Zhang, C.; Cao, X.; Wang, Z. L. Liquid-metal electrode for high-performance triboelectric nanogenerator at an instantaneous energy conversion efficiency of 70.6%. *Adv. Funct. Mater.* **2015**, *25*, 3718–3725.

[28] Jeon, S.-B.; Kim, D.; Seol, M.-L.; Park, S.-J.; Choi, Y.-K. 3-Dimensional broadband energy harvester based on internal hydrodynamic oscillation with a package structure. *Nano Energy* **2015**, *17*, 82–90.

[29] Kim, T.; Chung, J.; Kim, D. Y.; Moon, J. H.; Lee, S.; Cho, M.; Lee, S. H.; Lee, S. Design and optimization of rotating triboelectric nanogenerator by water electrification and inertia. *Nano Energy* **2016**, *27*, 340–351.

[30] Shi, Q. F.; Wang, H.; Wang, T.; Lee, C. Self-powered liquid triboelectric microfluidic sensor for pressure sensing and finger motion monitoring applications. *Nano Energy* **2016**, *30*, 450–459.

[31] Xi, Y.; Guo, H. Y.; Zi, Y. L.; Li, X. G.; Wang, J.; Deng, J.; Li, S. M.; Hu, C. G.; Cao, X.; Wang, Z. L. Multifunctional TENG for blue energy scavenging and self-powered wind-speed sensor. *Adv. Energy Mater.* **2017**, *7*, 1602397.

[32] Niu, S. M.; Liu, Y.; Wang, S. H.; Lin, L.; Zhou, Y. S.; Hu, Y. F.; Wang, Z. L. Theory of sliding-mode triboelectric nanogenerators. *Adv. Mater.* **2013**, *25*, 6184–6193.

[33] Li, Z. L.; Chen, J.; Guo, H. Y.; Fan, X.; Wen, Z.; Yeh, M.-H.; Yu, C. W.; Cao, X.; Wang, Z. L. Triboelectrification-enabled self-powered detection and removal of heavy metal ions in wastewater. *Adv. Mater.* **2016**, *28*, 2983–2991.

[34] Allred, A. L.; Rochow, E. G. A scale of electronegativity based on electrostatic force. *J. Inorg. Nuclear Chem.* **1958**, *5*, 264–268.